High-Pressure Transition of a Poly(ethylene glycol)-Grafted Phospholipid Monolayer at the Air/Water Interface

Valeria Tsukanova[†] and Christian Salesse*

Unité de Recherche en Ophtalmologie, Centre de Recherche du Centre Hospitalier de l'Université Laval CHUQ, Ste-Foy, Québec, Canada, G1V 4G2, and CERSIM, Université Laval, Ste-Foy, Québec, Canada G1K 7P4

Received October 28, 2002; Revised Manuscript Received May 8, 2003

ABSTRACT: Monolayer behavior of a poly(ethylene glycol)-grafted distearoylphosphatidylethanolamine with PEG molecular weight 5000 (DSPE−PEG5000) was studied by a variety of experimental methods. Slope changes in the surface pressure−molecular area ($\pi-A$) isotherm suggest two transitions in the DSPE−PEG5000 monolayer upon compression which were previously attributed to conformational changes in the polymeric moiety. However, comparative analysis of our experimental data implies that the second slope change in the isotherm at $\pi \approx 18$ mN/m originates from the monolayer collapse. As visualized by Brewster angle and atomic force (AFM) microscopy, the fluid homogeneous DSPE−PEG5000 monolayer is unable to sustain high pressures and collapses through vesicular structures formed as a result of 2D to 3D relaxation of an overcompressed film. AFM topographic images provided a height value of 9 nm for the collapsed structures on top of the monolayer, which can be referred to as the height of DSPE−PEG5000 lamellar structures. Thus, the collapse at a surprisingly low surface pressure implies that a distinct region where the PEG5000 moiety would adopt a brush conformation is probably never achieved for the DSPE−PEG5000 monolayer. Ellipsometric measurements of monolayer thickness confirm that although an elongated conformation is developed prior to the monolayer collapse, this conformation is better described as an "extended mushroom" rather than a "brush".

1. Introduction

Phospholipids with covalently attached poly(ethylene glycol) (PEG−phospholipids) have attracted considerable attention in recent years for both scientific and practical reasons. Indeed, PEG−phospholipids provide quite ideal model systems to study functional specialization of polymer−phospholipid conjugates in biological membranes,[1,2] structure of interfacial lipopolymer assemblies,[3,4] monolayer, bilayer, and liposome stability,[5−7] lateral organization in cell membranes,[2,4] and membrane fusion.[8] In addition to their fundamental scientific interest, they are also promising candidates for drug delivery since it was found that PEG−phospholipids provide stabilization of liposomal drug carriers and delivery systems.[5,9,10] When incorporated into supramolecular structures composed of native phospholipids, the bulky hydrophilic polymer moiety of PEG−phospholipids acts as a shield protecting the liposome surface.[5,6] Although the mechanism of stabilization is not fully understood yet, it is believed to originate from a complex interplay of the steric barrier created by PEG moiety and the net negative charge of incorporated PEG−phospholipids resulting in decreasing nonspecific adsorption of proteins and permeability of charged species.[1,5] To gain insight in processes involved in the stabilization mechanism, different aspects of interface behavior of PEG−phospholipids have been studied such as conformational changes in polymeric moiety in monolayers, bilayers, model membranes, vesicles, and liposomes,[3,5−7,11−14] partitioning of PEG−phospholipids in mixed monolayers and liposomal membranes,[1,3,7] polymer−polymer and polymer−lipid interactions in monolayers and bilayers,[3,7] hydration of PEG chains,[14] electrostatic properties of PEG-grafted interfaces,[1,5] and protein adsorption to PEG-grafted surfaces.[1,15]

Among others, two commercially available phosphatidylethanolamines N-derivatized in the headgroup with medium-sized poly(ethylene glycol)s of molecular weights 2000 (PEG2000) and 5000 (PEG5000) are commonly used for surface modification in biotechnological and biomedical areas.[1−6,9,10,15] Yet, despite drastically increasing number of studies, little is still known about the organization of these PEG−phospholipids at interfaces such as the air/water interface at which they show a complex phase behavior. In particular, surface pressure−molecular area ($\pi-A$) isotherms of both PEG2000- and PEG5000-grafted phosphatidylethanolamines suggest two transitions in the monolayers upon compression.[7] The first one shows up as a "pseudoplateau" at medium surface pressures. The second transition appears at higher surface pressures as a slope discontinuity in the low compressibility region of $\pi-A$ isotherms. While the plateau is usually attributed to conformational changes in the polymeric moiety,[3,7,12,13,16−20] the origin of the second transition is still rather unclear. On the basis of an assumption of the Alexander−de Gennes theory of tethered polymers, the low-compressibility region in PEG−phospholipid monolayer isotherms was generally associated with PEG chains in the highly stretched brush regime.[4,7,15,21] However, this interpretation has been recently questioned.[17,22−25] In particular, several studies on medium-sized grafted PEG chains showed that although the polymeric moiety tended to adopt a more elongated configuration with increasing surface density, this conformation could hardly be classified as "brush". It was better described as an "extended mushroom"[25] or a "pseudobrush".[12,14,16,18] Moreover, it was also pointed out that, for water soluble polymers such as PEGs, the high-energy barrier due to

* To whom correspondence should be addressed. E-mail: christian.salesse@crchul.ulval.ca.

[†] On leave from the Department of Chemistry, St. Petersburg State University, Petrodvorets, St. Petersburg 198904, Russia.

10.1021/ma0257806 CCC: $25.00
Published on Web 08/09/2003

excluded volume interactions between grafted chains makes it difficult to form very dense brushes with highly stretched polymeric chains at the air/water interface because some of the molecules will eventually dissolve in water in order to relax the stretching.[15,20,23,26] Therefore, the questions that have yet to be answered are whether (1) the low-compressibility region in PEG-grafted monolayer isotherms indeed corresponds to the polymeric chains in the highly stretched brush regime, (2) the discontinuity observed in the isotherm slope in the low-compressibility region has anything to do with conformational changes in the grafted chains, or (3) this second transition has different origins? For instance, on the basis of the infrared reflection adsorption spectroscopy data for a series of PEG−phospholipid monolayers, Baekmark et al.[17,21,22,27] proposed that it could also be due to a "native" transition associated with the pressure-induced ordering of aliphatic chains in the phospholipid part of lipopolymer molecules.

To better understand the organization of the PEG−phospholipids at the air/water interface, we attempted a systematic study of the monolayer behavior of a PEG-grafted phospholipid with PEG molecular weight 5000 using a variety of experimental methods. Comparative analysis of the $\pi-A$ isotherm, epifluorescence, and Brewster angle microscopy images, surface potential, and ellipsometry data provided new insight in the nature of the high-pressure transition that occurs in the low-compressibility region of the PEG-grafted monolayer isotherm. Complementary to epifluorescence and Brewster angle microscopy, atomic force microscopy was exploited to image defect formation and to investigate subtle details of monolayer microstructure.

2. Materials and Methods

2.1. Materials. The poly(ethylene glycol)-grafted phospholipid with PEG average molecular weight 5000, 1,2-distearoyl-*sn*-glycero-3-phosphatidylethanolamine-*N*-[poly(ethylene glycol) 5000] (DSPE−PEG5000), and the fluorescent probe, rhodamine−dioleoylphosphatidylethanolamine (DOPE−Rh) labeled at the headgroup (1,2-dioleoyl-*sn*-glycero-3-phosphatidylethanolamine-*N*-(lissamine rhodamine B sulfonyl)), were purchased from Avanti Polar Lipids and used without further purification. The chemical formula of the DSPE−PEG5000 molecule is presented in Figure 1. DSPE−PEG5000 monolayers were spread from chloroform solutions onto bare water surface. Spreading solutions of DSPE−PEG5000 were prepared at a concentration of 0.1−0.4 mg/mL and stored in the dark at 4 °C. Chloroform was of HPLC grade (Omega, QC). In all experiments, deionized water produced by a Nanopure water purification system was used as the subphase. The specific resistivity of water was 18×10^6 Ω·cm (pH 5.6 in equilibrium with atmospheric carbon dioxide).

2.2. Methods. A homemade Teflon-coated Langmuir trough with a movable barrier described elsewhere[28] was used to study PEG−phospholipid monolayers. The trough was thermostated and enclosed in a box. A filter paper Wilhelmy plate was used to measure surface pressure (π). Monolayer surface potential (ΔV) was detected with an ^{241}Am-coated ionizing electrode located 2 mm above the water surface while the reference electrode made of platinum was immersed at the bottom of the trough. During monolayer compression, π and ΔV were recorded simultaneously. Surface pressure was detected to an accuracy of ±0.1 mN/m while surface potential was measured to an accuracy of ±15 mV.

The trough was also interfaced with an epifluorescence microscope described previously.[29] To visualize the texture of the DSPE−PEG5000 monolayer, the fluorescent probe, DOPE−Rh, was added in concentration of 1 mol % to DSPE−PEG5000 spreading solutions. Epifluorescence micrographs were captured from different regions of the DSPE−PEG5000 isotherm. The filter set used to observe the probe fluorescence was a combination of a green excitation filter (Nikon, M 510-560, G-2A filter set), a dichroic mirror (Nikon, DM 580, G-2A filter set), and a barrier filter (Nikon, M 590, G-2A filter set). Excitation light was focused on the monolayer with a 20× objective (Nikon, MPlan 20).

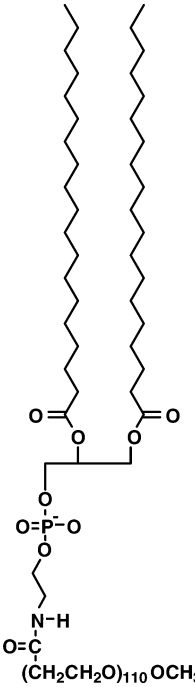

Figure 1. Chemical structure of the DSPE−PEG5000 molecule.

A commercial Brewster angle microscope (Nanofilm Technologie GmbH, Göttingen, Germany) was used for direct visualization of DSPE−PEG5000 monolayers at the air/water interface. The microscope was mounted on a NIMA film balance (Coventry, England). The frequency-doubled output of a Nd^{3+}:YAG-laser (532 nm, 20 mW) was used as the light source. The polarizer and analyzer were set to *p*-polarization. The air/monolayer/water interface was illuminated at an angle of 53.1°. Light was focused on the monolayer with a 10× objective (Nikon, MPlan 10). Monolayer compression and BAM measurements were made simultaneously.

Measurements of the thickness of DSPE−PEG5000 monolayers in situ at the air/water interface were performed using a homemade vibration-free Teflon-coated Langmuir trough interfaced with a conventional PCSA null ellipsometer. The trough was thermostated and enclosed in a box to minimize possible contamination of the air/monolayer/water interface. The ellipsometer described in detail elsewhere[30] was capable of tracking the azimuthal angles with a precision of 0.00034°. A 5-mW He−Ne laser operating at a wavelength of 632.8 nm was used as the light source. To record azimuthal angles, compression was stopped at a given surface pressure for 15−20 min.

Tapping mode atomic force microscopy (AFM) measurements were performed with a commercial Nanoscope IIIa (Digital Instruments, Santa Barbara, CA). Experiments were made in air at room temperature (20−25 °C) within 4 h after sample preparation. A 100×100 (x, y) $\times$ 2.5 (z) μm and a 5×5 (x, y) $\times$ 2.5 (z) μm scan ranges were typically used for imaging. Silicon tips (OTESP, Olympus, Nagano, Japan) with a bending spring constant of 0.12 N/m were used as received. The scan rate was 1 Hz. To eliminate artifacts, images were obtained from at least three macroscopically separated areas on each sample. All images were processed using the plane-fit and flatten procedures of Nanoscope IIIa software. To transfer DSPE−PEG5000 monolayers from the water surface onto a solid substrate, the Langmuir−Blodgett deposition

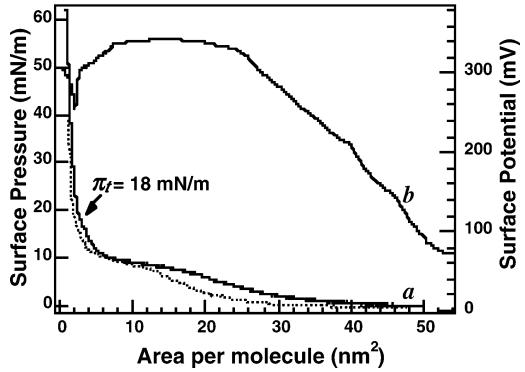

Figure 2. (a) $\pi-A$ and (b) $\Delta V-A$ isotherms of the DSPE−PEG5000 monolayer at the air/water interface. Dotted line shows hysteresis observed in the $\pi-A$ isotherm on expansion. The isotherms were measured at 20 ± 1 °C and a compression speed of 1.25 nm^2/molecule·min. The position of the high-pressure transition at $\pi \approx 18$ mN/m is indicated by the arrow.

technique was employed. Freshly cleaved mica was used as the deposition substrate. All monolayers were deposited in the upstroke mode. Depositions were done at various surface pressures in different regions of the DSPE−PEG5000 isotherm. The deposition pressure was held for 5 min prior to deposition to equilibrate the film. The deposition speed was 1 mm/min. The transfer ratios were close to unity for all depositions.

All experiments were done at 20 ± 1 °C, unless specified otherwise.

3. Results

3.1. Surface Pressure ($\pi-A$) and Surface Potential ($\Delta V-A$) Isotherms. Figure 2 shows the $\pi-A$ isotherm of the DSPE−PEG5000 monolayer on pure water. Typical of molecules bearing a bulky hydrophilic polymer moiety, the DSPE−PEG5000 monolayer exhibits the expanded type isotherm.[31,32] Indeed, surface pressure is detectable at fairly large molecular areas, gradually increases with decreasing molecular area, and reaches a plateau value below 18 nm^2/molecule. The plateau extends to an area of ∼5 nm^2/molecule at a surface pressure of approximately 8.6 mN/m. Upon further compression, a region of low compressibility with rapidly increasing π is attained. Yet, another discontinuity occurs in the slope of the isotherm in the 3.2−2.4 nm^2/molecule region. This second plateaulike region is more clearly demonstrated by the portion of the DSPE−PEG5000 isotherm above the plateau shown on a larger scale in Figure 3A and by the plot of lateral area compressibility as a function of the reciprocal of molecular area in Figure 3B. The second transition is observed at π of approximately 18 mN/m that is slightly higher than the isotherm plateau pressure and, consequently, can be referred to as the high-pressure transition. This isotherm is similar to previously reported data.[7,27]

Distinct regions corresponding to the slope changes in the $\pi-A$ isotherm are distinguished in the $\Delta V-A$ isotherm of the DSPE−PEG5000 monolayer presented in Figure 2 (curve b). Surface potential increases gradually in the 50−25 nm^2/molecule region reaching a maximum value of +360 mV at a plateau that extends to 8 nm^2/ molecule. On further compression, ΔV decreases slowly and a sudden drop is detected at an area of approximately 2.2 nm^2/molecule while below 1.4 nm^2/molecule ΔV increases again.

3.2. Epifluorescence and Brewster Angle Microscopy Studies. Epifluorescence micrographs captured from a DSPE−PEG5000 monolayer at the air/water interface display continuous fluorescent fields from low surface pressures up to the point of monolayer collapse. As seen in Figure 4, the images became progressively brighter upon compression while no special features were observed. Similarly to the fluorescence micrographs, BAM images of a DSPE−PEG5000 monolayer remained homogeneous for a large range of molecular areas. A featureless gray pattern seen in Figure 5A was typical of images taken in the 50−5 nm^2/molecule region of the $\pi-A$ isotherm. However, by contrast to the fluorescence micrographs, an abrupt change was observed in the BAM images taken above the plateau of the $\pi-A$ isotherm. As seen in Figure 5B, bright grains appeared in the field for the first time when the monolayer was compressed to $A \approx 4$ nm^2/molecule ($\pi \approx$ 13.6 mN/m). Interestingly, while the number of grains increased progressively as the monolayer was compressed across the 4−2.5 nm^2/molecule region (between the plateau at $\pi \approx$ 8.6 mN/m and the high-pressure transition at $\pi \approx 18$ mN/m), their average size decreased markedly. Eventually, the entire field was covered with the bright phase at areas below 2.3 nm^2/molecule ($\pi \approx$ 18.9 mN/m). The monolayer showed a porous appearance since most of the individual small grains did not coalesce even at high surface pressures. The average size of the grains decreased from ∼13 (Figure 5B) to 5 μm (Figure 5C) in diameter while a few large bright grains that scatter significantly the incident light appeared in the BAM image taken at the end of the high-pressure transition (Figure 5C).

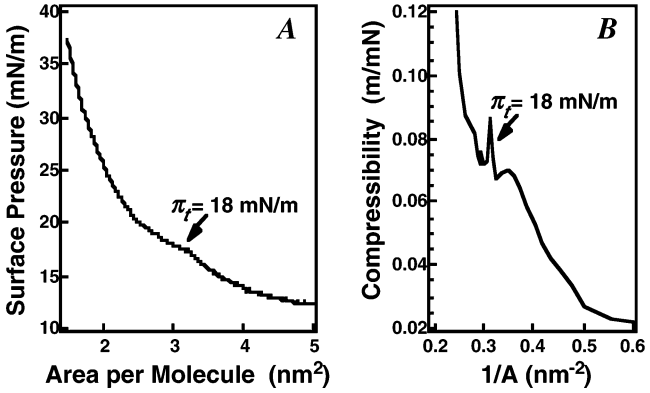

Figure 3. (A) Enlarged portion of the $\pi-A$ isotherm in the low-compressibility region featuring a plateau at $\pi \approx 18$ mN/m and (B) the plot of lateral area compressibility, C, as a function of reciprocal of molecular area, $1/A$. The compressibility was calculated from the slope of $\pi-A$ isotherm as given by $C = -(1/A)(\partial A/\partial \pi)_T$.[53] The plot shows a first-order transition in a molecular area range of 3.2−2.4 nm^2/molecule at a surface pressure of 18 mN/m.

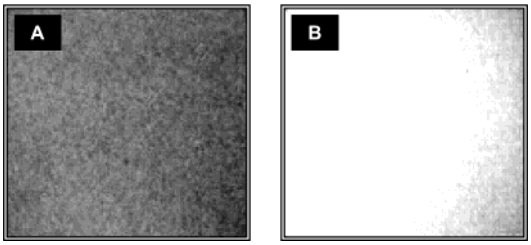

Figure 4. Fluorescence micrographs of a DSPE−PEG5000 monolayer at the air/water interface: (A) $\pi = 4.1$ mN/m, $A =$ 25 nm^2/molecule; (B) $\pi = 18.9$ mN/m, $A = 2.3$ nm^2/molecule.

3.3. Ellipsometric Measurements. Thickness of the DSPE−PEG5000 monolayer at the air/water interface

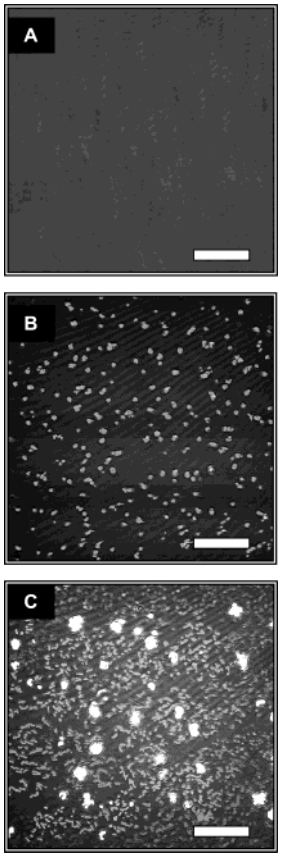

Figure 5. BAM images captured from a DSPE−PEG5000 monolayer at the air/water interface above the $\pi-A$ isotherm plateau: (A) $\pi = 11.2$ mN/m, $A = 5$ nm^2/molecule; (B) $\pi = 13.6$ mN/m, $A = 4$ nm^2/molecule; (C) $\pi = 18.9$ mN/m, $A = 2.3$ nm^2/molecule. Scale bar = 100 μm.

was assessed by ellipsometry. At a fixed angle of incidence and wavelength, ellipsometry measures simultaneously two parameters, i.e., the angles Ψ (the change in the amplitude ratio due to reflection) and Δ (the relative phase shift). Deviations of the two ellipsometric angles from the values for $\bar{\Psi}$ and $\bar{\Delta}$ of the bare water surface ($\delta\Psi = \Psi - \bar{\Psi}$ and $\delta\Delta = \Delta - \bar{\Delta}$) are related to the refractive index n and thickness d of the film.[30−33] In our experiments, a novel technique was employed to determine the ellipsometric angles Ψ and Δ with high accuracy. It has been shown[30] that precise absolute Ψ and Δ allow n to be separated from d by a numerical inversion procedure. Thus, the film thickness, d, was calculated using a polynomial approach explained in detail elsewhere[30] which gives the solution for both n and d directly from the ellipsometric equations and experimental values of Ψ and Δ.

Table 1 shows values of n and d for the DSPE−PEG5000 monolayer at the air/water interface obtained at different molecular areas. As seen in the table, above 35 nm^2/molecule the monolayer thickness remained unchanged. The value of approximately 0.9 nm agrees well with values reported previously for expanded monolayers of PEOs.[31,33,34] Then, below 30 nm^2/molecule the monolayer thickness starts to increase gradually. At the end of the isotherm plateau, thickness was found in a range of 6.1−6.8 nm. By contrast, above the plateau, slightly reducing molecular area induced significant changes in d. As seen in Table 1, a value as high as 15.8 nm was eventually attained at 1.2 nm^2/molecule.

Table 1. Refractive Index and Film Thickness Obtained for DSPE−PEG5000 from the ψ and Δ Angles Using the 5th Degree Polynomial Approach[30]

A (nm^2)	π (mN/m)	n_1	d_1 (nm)
above 35		1.3601	0.9 ± 0.2[a]
28	2.6	1.3609	1.8 ± 0.3
18.5	6.7	1.3630	3.3 ± 0.3
9	9.3	1.3650	5.2 ± 0.3
7.7	9.7	1.3669	6.1 ± 0.3
6.5	10.1	1.3676	6.4 ± 0.5
5	11.2	1.3685	6.8 ± 0.5
4	13.6	1.3698	8.8 ± 0.1
3	17.3	1.3738	10.1 ± 0.1
2	25.3	1.3792	12.6 ± 0.1
1.2	48.4	1.3882	15.8 ± 0.1

[a] The standard deviation was calculated on the basis of a series of measurements made with three different monolayers.

3.4. Atomic Force Microscopy of DSPE−PEG5000 Monolayers Transferred onto Solid Substrate. Although epifluorescence microscopy and BAM allowed visualization of the monolayer morphology in situ at the air/water interface, these methods have a lateral resolution limited to ~1 μm. A nanometer-scale lateral and normal resolution was achieved with AFM, thus providing a much more detailed picture of the molecular reorganization in the monolayer upon compression. However, AFM required the monolayer to be transferred onto a solid substrate. In some cases, the original structure of the film may be lost during the transfer process.[35] In our study, AFM images of transferred DSPE−PEG5000 films were consistent with BAM images captured from a monolayer at the air/water interface at the same surface pressures. Indeed, similar to epifluorescence and BAM data for monolayers on water surface, AFM performed with DSPE−PEG5000 monolayers transferred onto mica at various surface pressures showed that a homogeneous phase exhibiting a small height difference existed in the 50−5 nm^2/molecule region of the $\pi-A$ isotherm. The uniform topographic image presented in Figure 6 was typical of DSPE−PEG5000 monolayer from low surface pressures up to the end of the isotherm plateau. Then, phase separation is clearly observed in AFM images of films deposited at surface pressures above 12 mN/m (in the low-compressibility region of the isotherm). As seen in Figure 7A, the film deposited at $\pi = 13.6$ mN/m and $A = 4$ nm^2/molecule is made of elevated features (bright phase), embedded in a continuous matrix (dark phase). The step height measured between the two phases is ~9 nm. The elevated structures do not show any regular shape or size and are randomly distributed throughout the field. Closer look at these elevated structures in the deposited film using topography scan 5 × 5 μm enabled us to visualize a fine structure composed of numerous defects in the form of holes (Figure 7B). The height difference measured from the cross sections in the topographic image in Figure 7 shows that the holes have a rather uniform depth of 8−9 nm. Furthermore, in analogy to the BAM images, a striking transformation into another structure was observed upon further compression below 3 nm^2/molecule. Figure 8A shows an AFM image of a film deposited at a surface pressure of 18.9 mN/m, slightly above the high-pressure transition in the DSPE−PEG5000 isotherm. In a comparison of the images in Figures 7A and 8A, an interesting observation was made. While the elevated features in films deposited at $12 \leq \pi \leq 17$ mN/m appeared agglomerated in the form of distant islands (Figure 7A),

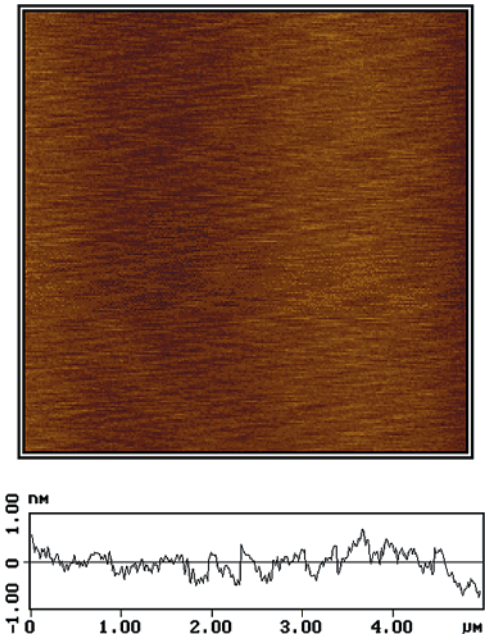

Figure 6. Topography AFM image of a DSPE−PEG5000 monolayer deposited on mica at $\pi = 11.2$ mN/m ($A = 5$ nm^2/molecule). A section analysis for the topography image shows a small height difference throughout the film.

a morphology that resembles a large-scale liquid-crystalline network was discovered in DSPE−PEG5000 films deposited at higher surface pressures (Figure 8A). At the same time, the 5 × 5 μm topography scan in Figure 8B shows that the fine structure within the liquid-crystalline network is almost identical with that in Figure 7B except for some inhomogeneities that are clearly seen in the bright phase. Thus, similar morphology changes revealed by both AFM and BAM imply that the local molecular organization, size, and distribution of the elevated features in transferred films were almost identical with those in monolayers formed initially on water. Therefore, we believe that conclusions about the structure and molecular ordering derived from the AFM study for transferred films are valid for the DSPE−PEG5000 monolayer at the air/water interface as well.

4. Discussion

A number of studies have shown that both PEOs and a vast majority of PEG-grafted phospholipids readily spread at the air/water interface forming stable monolayers.[5,7,13,14,31−34] As reflected by the expanded-type $\pi-A$ isotherm shown in Figure 2, the monolayer behavior of DSPE−PEG5000 is profoundly influenced by the presence of the PEG moiety in the phospholipid structure. Furthermore, two transitions are suggested by changes in the slope of the isotherm. The first one appears as the extended plateau at $\pi \approx 8.6$ mN/m while the second one is marked by the slope discontinuity in the low-compressibility region of the isotherm at $\pi \approx$ 18 mN/m.

The plateau in $\pi-A$ isotherms of PEO- and PEG-grafted monolayers at the air/water interface is usually attributed to conformational changes in polymeric moiety.[3,7,12,13,16−20] In particular, for PEOs and PEGs that are in good solvent conditions at the air/water interface,[36] the plateau can be interpreted as a first-order transition from pancake to brush conformation predicted by Alexander.[12,13,15,16,18−20,26] Indeed, BAM study performed with a polysterene−PEO diblock co-

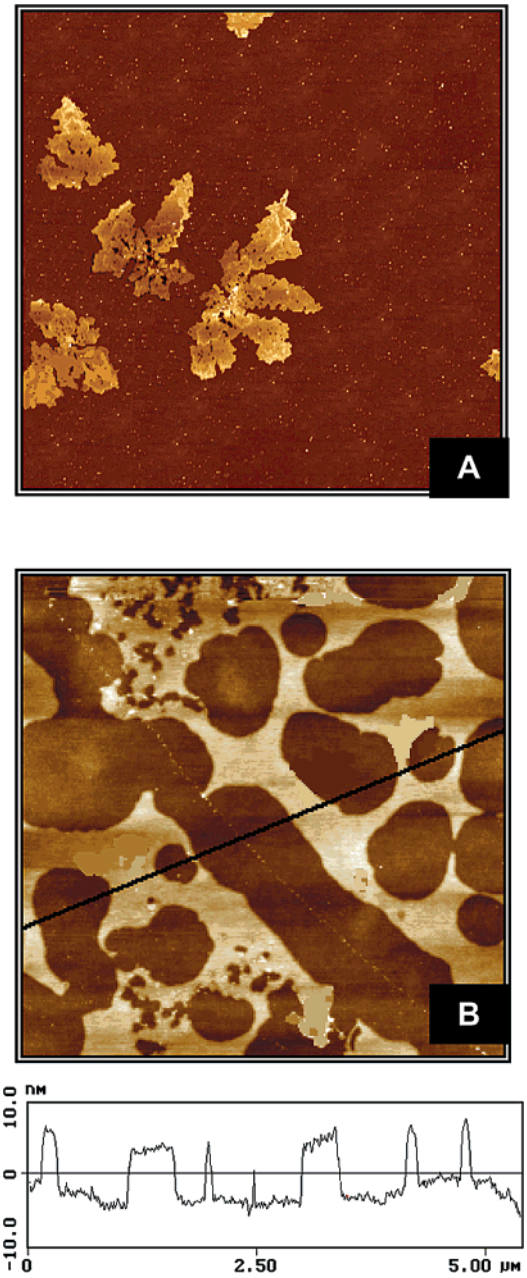

Figure 7. Topography AFM image of a DSPE−PEG5000 monolayer deposited on mica at $\pi = 13.6$ mN/m ($A = 4$ nm^2/molecule). The gray scale indicates the height of features; higher levels appear lighter in the image while lower ones are dark. Key: (A) 100 × 100 (x, y) μm scan; (B) 5 × 5 (x, y) μm scan performed to visualize fine structure within the bright phase. A section analysis along the black line in image B shows that the step height between higher and lower levels is ∼8−9 nm.

polymer bearing a long PEO chain (degree of polymerization, $n \approx 700$) revealed the coexistence of pancake regimes and brushes in the isotherm plateau.[13] On the other hand, it was reported that BAM failed to visualize the coexistence of these two phases for monolayers grafted with medium-sized PEO or PEG chains ($45 \leq n \leq 400$).[13,19] Neither did our BAM study show any sigh of phase coexistence in the plateau of DSPE−PEG5000 isotherm (see Figure 5A). Moreover, the analysis of surface pressure data for DSPE−PEG5000 revealed the lack of a clear-cut peak in the plot of lateral area compressibility near the plateau onset thus implying that the plateau cannot be ascribed to a first-order

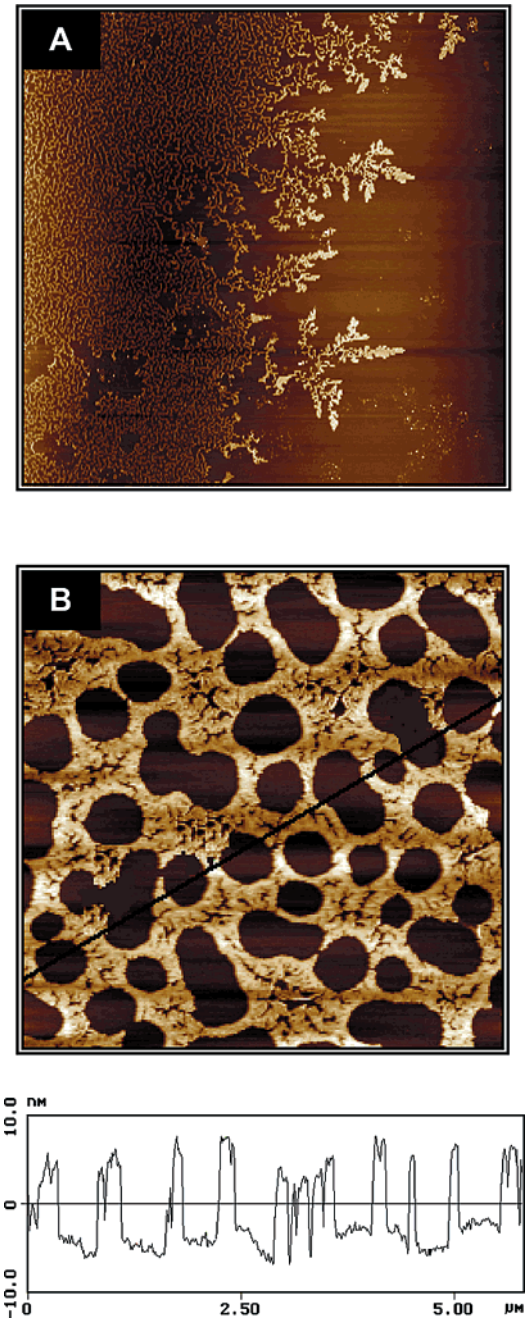

Figure 8. Topography AFM image of a DSPE−PEG5000 monolayer deposited on mica at $\pi = 18.9$ mN/m ($A = 2.3$ nm^2/molecule). The gray scale is the same as in Figure 7. Key: (A) 100 × 100 (x, y) μm scan; (B) A 5 × 5 (x, y) μm scan performed to visualize fine structure within the bright phase. A section analysis along the black line in image B shows that the step height between higher and lower levels is ∼9 nm.

phase transition.[7] The hypothesis of PEG5000 brush formation in the plateau region of DSPE−PEG5000 isotherm is further confronted by our ellipsometric data. Indeed, as seen in Table 1, a value of 6.8 nm was obtained for the monolayer thickness at an area of 5 nm^2/molecule (at the end of the isotherm plateau). This value is too small compared to the predictions of scaling approaches for the height of the PEG5000 brush usually found in a range of 10−12.5 nm.[4,6,21] Therefore, the lack of the two major properties of first-order transitions together with the small thickness values makes the interpretation of the DSPE−PEG5000 isotherm plateau in terms of the Alexander concept rather doubtful. An alternative interpretation suggested in the literature attributes the plateau to the pancake-to-mushroom conformational transition.[7,17,27] This transition however is not well-defined theoretically, and no experimental evidence has been presented to support this concept. Nevertheless, the thickness value of 6.8 nm measured by ellipsometry that slightly exceeds the three-dimensional radius of gyration, R_g, of PEG5000 moiety may be considered as an indication of PEG5000 mushroom formation at the end of the isotherm plateau since the thickness of a polymer layer is scaled by R_g if the layer is in the mushroom regime.[7,37,38] In a good solvent, the polymer radius of gyration is

$$R_g = an^{0.6} \quad (1)$$

where a is the monomer length and n is the degree of polymerization.[6,25,38] With $a = 0.35$ nm[6,25] and $n = 110$, eq 1 yields $R_g = 5.8$ nm. This value is indeed comparable with the thickness of DSPE−PEG5000 monolayer found in a range of 5.2−6.8 nm at the end of the isotherm plateau. However, the analysis of π−A isotherm and ellipsometric data in terms of radii of gyration of PEG5000 moiety in the monolayer plane, $R_{g,xy}$, and along the interface normal, $R_{g,z}$, suggests that the average conformation developed at the end of the DSPE−PEG5000 isotherm plateau differs from the hemispherical mushroom described by de Gennes.[38] For instance, in a comparison of the radius of gyration in the monolayer plane, $3.2 \leq R_{g,xy} \leq 2.5$ nm (as inferred from the isotherm), to that along the interface normal, $6.1 \leq R_{g,z} \leq 6.8$ (ellipsometric data) for the PEG5000 moiety in the 7.7−5 nm^2/molecule region, the extension of the polymeric chain into the subphase was found some 2- to 3-fold greater than that in the monolayer plane. Such a configuration can be described as an "extended mushroom" or "pseudobrush".[12,14,16,18,25] At this point, we therefore may conclude that although less extended than brushes, a relatively elongated conformation is developed at the end of the DSPE−PEG5000 isotherm plateau. The nature of this transition will be discussed in detail in our forthcoming paper. In this report, our further discussion will be focused mainly on the second transition that appears as the discontinuity in the isotherm slope at $\pi \approx 18$ mN/m.

As mentioned above, the origin of the second transition in the DSPE−PEG5000 isotherm is even more uncertain. In a vast majority of studies, the interpretation of conformational changes in PEG chains grafted at the interfaces is based on an a priori assumption that at high surface densities the chains should stretch into brushes.[1−7,11−16,18−21,26,37] In particular, for DSPE−PEG5000 monolayer at the air/water interface, it was assumed that the low-compressibility region in its isotherm corresponds to PEG5000 chains in the highly stretched brush regime.[4,7,15,21] However, some concerns have been raised on whether the models that were initially developed for polymeric chains grafted onto solid surfaces are adequate in describing the polymer-grafted monolayers at the air/water interface.[15,23,24] Given the penetrable nature of the air/water interface, cohesive interactions between relatively short aliphatic chains (compared to the size of PEG moiety) pinning PEG−phospholipid conjugates to the interface may not be strong enough to compensate for steric repulsion between stretching PEG chains that tends to squeeze some of the molecules out of the monolayer to relax the

stretching.[15,26] As a result, with increasing surface density, the monolayer collapse is likely to set in before the highly stretched brush regime is reached.[15,23,26] Therefore, the question that still remains is whether the PEG5000 chains indeed continue to stretch into the subphase upon compression above the plateau? On one hand, the results of neutron and X-ray reflectivity studies performed with DSPE−PEG5000 at the air/water interface indicated formation of a dense and thick polymer layer in the low-compressibility region of the isotherm.[4,21] Ellipsometric data obtained in the present study also showed a sudden increase in monolayer thickness above the DSPE−PEG5000 isotherm plateau. In the 4−1.2 nm^2/molecule region, monolayer thickness was found in a range of 8.8−15.8 nm which correlates well with the previously reported neutron and X-ray reflectivity data.[4,21] Because the values of 8.8−15.8 nm obtained in the low-compressibility region are in good agreement with the theoretical predictions of scaling theories for the height of PEG5000 brush, these values were attributed to the stretching of polymeric chains at high surface pressures and formation of PEG5000 brushes at the air/water interface.[4,21] On the other hand, for polymeric systems, a thickening of a layer resulting from the stretching of polymeric chains can be mistaken with an increase in thickness due to monolayer collapse, if thickness measurements alone are considered to distinguish which scenario is more likely. On the basis of a comparative analysis of surface pressure, surface potential, ellipsometry, BAM, and AFM data, we argue that the abrupt increase in monolayer thickness observed in the low-compressibility region of the $\pi-A$ isotherm is caused by the formation of collapsed structures in an overcompressed DSPE−PEG5000 monolayer as discussed below.

According to the theoretical concepts suggested in the literature to describe conformational transitions in grafted polymeric chains, for medium-sized chains, the transition from "extended mushroom" conformation to brushes is not expected to be sharp.[37] Although the theories predict a rapid increase in surface pressure and monolayer thickness, no plateau should be observed in $\pi-A$ isotherms as a result of this transition. By contrast, the slope discontinuity in the low-compressibility region at $\pi \approx 18$ mN/m appears to be the second plateaulike region in the DSPE−PEG5000 isotherm. As seen in Figure 3A, surface pressure does level off at an area of ~3.2 nm^2/molecule, and the plateau extends to ~2.4 nm^2/molecule. Although the plateau is not horizontal, the plot of lateral area compressibility in Figure 3B suggests that it is a first-order transition plateau. This finding implies that the stretching of PEG5000 chains into brushes, if it occurs at all, is obviously not a major process taking place in the low-compressibility region of the DSPE−PEG5000 isotherm.

Given an indication of a first-order phase transition, Baekmark et al., Ahrens et al., and Wiesenthal et al. associated the high-pressure plateau with a pressure-induced ordering of the aliphatic chains in the phospholipid part of the DSPE−PEG5000 molecule analogous to the liquid-expanded−liquid-condensed (LE−LC) phase transition in phospholipid monolayers.[17,21,22,27] Yet, this ordering in PEG-grafted phospholipid monolayers was expected to occur on a somewhat smaller scale. The authors predicted formation of ordered phase domains 6−10 nm in diameter.[21] As discussed above, on approach of the high-pressure transition plateau in the DSPE−PEG5000 isotherm, domains indeed start to appear in both AFM and BAM images. However, the size of the domains is found in a range of 5−13 μm, i.e., orders of magnitude larger than that predicted by Ahrens et al.[21] In general, bright grains seen in BAM images in Figure 5B,C indicate regions of greater film density or thickness and may be attributed to either nuclei of LC phase[39,40] or buckling collapsed structures.[40−43] To find out whether these domains represent an ordered phase analogous to LC phases in phospholipid monolayers, we performed epifluorescence microscopy study. Since epifluorescence microscopy is based on different partitioning of fluorescent probe into ordered and disordered regions, LC phase domains that usually appear bright in BAM (as they have a greater optical thickness than the surrounding film) are supposed to be dark in epifluorescence micrographs because the probe used in our study, DOPE−Rh, has high affinity for LE phases and is largely excluded from LC phases.[44] Hence, if the two phases coexisted in the DSPE−PEG5000 monolayer, exclusion of the probe from the LC phase would immediately result in the appearance of dark domains in epifluorescence micrographs. The epifluorescence micrographs in Figure 4 however display a uniform phase that features no morphological changes throughout the entire isotherm thus ruling out the hypothesis of LC-like phase domain formation in the DSPE−PEG5000 monolayer at the air/water interface. Given also the fact that the bright grains appearing in BAM images in the low-compressibility region of the DSPE−PEG5000 isotherm give rise to light scattering as compression proceeds (see Figure 5C), these grains seem more likely to be elevations formed on top of the monolayer. Moreover, AFM images of DSPE−PEG5000 monolayers transferred on mica exhibit similar elevated features whose distribution and size are almost identical to those of bright grains observed with BAM in DSPE−PEG5000 monolayers at the air/water interface as discussed above. This enables us to attribute the grainy-textured bright phase in Figure 5B and C to budding collapsed structures.

Recent epifluorescence microscopy,[42,44,45] BAM,[40,42,44] scanning probe microscopy,[42] and light scattering microscopy[45] studies have also shown evidence for the formation of 3D defects and discontinuities in a number of monolayers at the air/water interface as a potential mode of relaxation of overcompressed films. For some monolayer systems, the formation of 3D defects was observed at surprisingly low surface pressures.[46] As the collapsed structures remain attached to the monolayer, this type of collapse leads to the coexistence of "phases" corresponding to a 2D monolayer and 3D collapsed fragments at the air/water interface thus resembling an equilibrium first-order phase transition.[42,46] Macroscopically, it should show up as a plateaulike region in the $\pi-A$ isotherm where the lateral compressibility, C, diverges because extra area can be pulled out of the monolayer without resistance.[46] This is thus in good agreement with the surface pressure data presented in Figure 3. The drop in surface potential detected at an area of ~2.2 nm^2/molecule ($\pi \approx 25$ mN/m; see curve b, Figure 2) is also likely to result from the formation of collapsed fragments in monolayer.[47,48] Moreover, the DSPE−PEG5000 isotherm exhibits a surface pressure dependent hysteresis. Repeated compression−expansion circles showed reversible behavior up to 12 mN/m while noticeable hysteresis loops were recorded upon decom-

pression started above the high-pressure transition (dotted line in Figure 2). A similar behavior was previously observed for some PEO−lipid conjugates[26] as well as for other polymers[32,34,49−51] and was also attributed to monolayer collapse. For PEOs and PEO−lipid conjugates, collapse pressures were previously reported in a range of 10−16 mN/m.[12,26,34] Interestingly, surface pressure at which the plateau corresponding to monolayer collapse occurs was found to vary with the length of hydrophobic anchors on PEO−lipid conjugates. Higher π values were reported for longer aliphatic chains. In particular, for a PEO chain with $n = 135$ bearing two C_{12} aliphatic anchors, the collapse plateau was observed at $\pi \approx 15$ mN/m.[26] Appearance of a collapse plateau in the isotherm of DSPE−PEG5000 bearing longer aliphatic chains (C_{18}) at $\pi \approx 18$ mN/m is therefore in keeping with the observed trend. Furthermore, the 2D to 3D relaxation phenomenon may occur via either a large-scale folding or micron-scale vesiculation.[42,46] According to Gopal et al.,[42] the collapse mode correlates with the reological properties and morphology of the monolayer prior to collapse. For instance, homogeneous fluid (or less rigid) monolayers may not be able to sustain large-scale folding. Instead, they are likely to collapse through vesicular structures, which are either pulled into the subphase or curled up on top of the monolayer.[42] Therefore, the hypothesis of the collapse via vesiculation seems very consistent with the experimental data obtained for the DSPE−PEG5000 monolayer in the present study.

It should be pointed out however that by using the term "vesicular structures" we refer to the morphological shape of collapsed fragments rather than to their actual structure. At this point, we can only make some speculative conclusions about the structural organization within the collapsed fragments on the basis of the analysis of AFM images. AFM study using a 5×5 μm topography scan revealed a fine structure within the collapsed fragments formed on top of the monolayer at $\pi > 12$ mN/m which is made of smaller grains fused into an entire lacelike network (see Figures 7B and 8B). Similar periodic globular structures were observed in collapsed phospholipid monolayers[42] and in films of diblock copolymers.[52] These collapsed structures are believed to be lamellar.[42,52] In general, since the thickness of a monolayer is smaller than the thickness of a lamella, elevated features with a step height which corresponds to the thickness of lamellar structure[52] will be formed on top of the monolayer when laterally ordered lamellar microdomains occur as a result of 2D to 3D relaxation of an overcompressed film. Hence, the height difference of approximately 9 nm, as measured from the cross sections in the AFM topographic images in Figures 7 and 8, can be referred to the height of lamellar structures formed by DSPE−PEG5000 molecules. Further estimate of the lateral dimensions of these structures shows that the height of DSPE−PEG5000 lamellar microdomains is approximately two times smaller than the in-plane diameter which was found ~18 nm for the smallest objects in AFM images.

Concluding our discussion, we emphasize the important finding made above that the DSPE−PEG5000 monolayer collapses at $\pi \approx 18$ mN/m corresponding to the high-pressure transition in its $\pi-A$ isotherm. In fact, first signs of collapse appear in BAM images at a surface pressure as low as ~13.6 mN/m (Figure 5B). This suggests that a distinct region where the PEG5000 moiety would adopt a highly stretched brush conformation is probably never achieved for the DSPE−PEG5000 monolayer. By the same token, it seems unlikely that PEG5000 brushes can be formed at the air/water interface by simply reducing the area available/DSPE−PEG5000 molecule in the monolayer. Although the stretching of PEG5000 chains into the subphase does increase with decreasing molecular area in 35−5 nm^2/molecule region as indicated by the measurements of monolayer thickness (Table 1), compression in the low-compressibility region has little or no effect at all on the PEG5000 chain conformation since the monolayer collapses by contrast to the stretching of PEG5000 chains into highly extended brushes assumed in a vast majority of studies. The stretching of PEG5000 chains at the air/water interface therefore seems limited. In particular, for DSPE−PEG5000, the limit of "stretching regime" can be roughly estimated from our data as ~5 nm^2/molecule. Further decrease in molecular area will immediately destabilize the monolayer. Interestingly, by contrast to what one might assume,[15,26] DSPE−PEG5000 molecules do not dissolve into the subphase upon the monolayer collapse. Instead, the collapsed structures stay attached to the monolayer. We believe that this may also have implications for PEG-grafted lipid membranes. Indeed, our finding implies that an unlimited increase in PEG5000 grafting density may result in local elastic deformations of the surface layer and thus decrease the stability of such systems as monolayers, bilayers, and liposomal membranes rather than provide the desired steric stabilization.

Conclusions

Monolayer behavior of a poly(ethylene glycol)-grafted distearoylphosphatidylethanolamine with PEG molecular weight 5000, DSPE−PEG5000, was studied using a variety of experimental methods. Comparative analysis of the $\pi-A$ and $\Delta V-A$ isotherms, ellipsometry, epifluorescence, and Brewster angle microscopy data provided a new insight into the nature of high-pressure transition in the DSPE−PEG5000 monolayer. The appearance of disordered vesicular structures on top of the monolayer in BAM images together with $\pi-A$ isotherm hysteresis observed in the low-compressibility region, drop in ΔV, and abrupt increase in monolayer thickness indicates that the DSPE−PEG5000 monolayer collapses at $\pi \approx 18$ mN/m corresponding to the high-pressure transition in its isotherm. Atomic force microscopy study performed with DSPE−PEG5000 films transferred on mica confirms that elevated structures appear in the monolayer on approaching the high-pressure transition plateau. Topographic images provided a height value of 9 nm for these structures which can be referred to as the height of DSPE−PEG5000 lamellar structures formed as a result of 2D to 3D relaxation of an overcompressed monolayer. Thus, the collapse at a surprisingly low surface pressure enabled us to conclude that a distinct region where the PEG5000 moiety would adopt a brush conformation is probably never achieved for the DSPE−PEG5000 monolayer. Indeed, ellipsometric measurements of the monolayer thickness showed that although an elongated conformation was developed prior to the monolayer collapse, this conformation is better described as an "extended mushroom" rather than a "brush".

Acknowledgment. The authors thank the Natural Sciences and Engineering Research Council of Canada

for the financial support of this study. C.S. is a chercheur boursier national of the Fonds de recherche en santé du Québec. An invitation fellowship of the Centre de Recherche en Sciences et Ingénierie des Macromolécules (Quebec, Canada) to V.T. is gratefully acknowledged. We are grateful to P. Basque and A. Nabet for the scanning and processing of AFM images. We also thank Dr. D. Ducharme for his collaboration in the ellipsometric experiments and S. Senkow for helping out with the preparation of deposited films.

References and Notes

(1) Efremova, N. V.; Bondurant, B.; O'Brien, D. F.; Leckband, D. E. *Biochemistry* **2000**, *39*, 3441.
(2) Rostovtseva, T. K.; Nestorovich, E. M.; Bezrukov, S. M. *Biophys. J.* **2002**, *82*, 160.
(3) Majewski, J.; Kuhl, T. L.; Gerstenberg, M. C.; Israelachvili, J. N.; Smith, G. S. *J. Phys. Chem. B* **1997**, *101*, 3122.
(4) Bianco-Peled, H.; Dori, Y.; Schneider, J.; Sung, L.-P.; Satija, S.; Tirrell, M. *Langmuir* **2001**, *17*, 6931.
(5) Kuhl, T. L.; Leckband, D. E.; Lasic, D. D.; Israelachvili, J. N. *Biophys. J.* **1994**, *66*, 1479.
(6) Kenworthy, A. K.; Hristova, K.; Needham, D.; McIntosh, T. J. *Biophys. J.* **1995**, *68*, 1921.
(7) Baekmark, T. R.; Elender, G.; Lasic, D. D.; Sackmann, E. *Langmuir* **1995**, *11*, 3975.
(8) Lentz, B. R. *Chem. Phys. Lipids* **1994**, *73*, 91.
(9) Bhadra, D.; Bhadra, S.; Jain, P.; Jain, N. K. *Pharmazie* **2002**, *57*, 5.
(10) Harris, J. M.; Martin, N. E.; Modi, M. *Clin. Pharmacokinet.* **2001**, *40*, 539.
(11) Fauré, M. C.; Bassereau, P.; Desbat, B. *Eur. Phys. J. E* **2000**, *2*, 145.
(12) Fauré, M. C.; Bassereau, P.; Carignano, M. A.; Szleifer, I.; Gallot, Y.; Andelnam, D. *Eur. Phys. J. B* **1998**, *3*, 365.
(13) Fauré, M. C.; Bassereau, P.; Lee, L. T.; Menelle, A.; Lheveder, C. *Macromolecules* **1999**, *32*, 8538.
(14) Kitano, H.; Ichikawa, K.; Ide, M.; Fukuda, M.; Mizuno, W. *Langmuir* **2001**, *17*, 1889.
(15) Vermette, P.; Meagher, L. *Colloids Surf., B* **2003**, *28*, 153.
(16) Fauré, M. C.; Bassereau, P.; Carignano, M. A.; Szleifer, I.; Gallot, Y.; Andelnam, D. *Eur. Phys. J. E* **2000**, *2*, 145.
(17) Baekmark, T. R.; Wiesenthal, T.; Kuhn, P.; Albersdörfer, A.; Nuyken, O.; Merkel, R. *Langmuir* **1999**, *15*, 3616.
(18) Gonçalves da Silva, A. M.; Filipe, E. J. M.; d'Oliveira, J. M. R.; Martinho, J. M. G. *Langmuir* **1996**, *12*, 6547.
(19) Bijsterbosch, H. D.; de Haan, V. O.; de Graaf, A. W.; Mellema, M.; Leermakers, F. A. M.; Cohen Stuart, M. A.; van Well, A. A. *Langmuir* **1995**, *11*, 4467.
(20) Zhao, H.; Dubielecka, P. M.; Söderlund, T.; Kinnunen, P. K. J. *Biophys. J.* **2002**, *83*, 954.
(21) Ahrens, H.; Baekmark, T. R.; Merkel, R.; Schmitt, J.; Graf, K.; Raiteri, R.; Helm, C. A. *Chemphyschem* **2000**, *2*, 101.
(22) Baekmark, T. R.; Wiesenthal, T.; Kuhn, P.; Bayerl, T. M.; Nuyken, O.; Merkel, R. *Langmuir* **1997**, *13*, 5521.
(23) Richards, R. W.; Rochford, B. R.; Webster, J. R. P. *Polymer* **1997**, *38*, 1169.
(24) Cox, J. K.; Yu, K.; Constantine, B.; Eisenberg, A.; Lennox, R. B. *Langmuir* **1999**, *15*, 7714.
(25) Rex, S.; Zuckermann, M. J.; Lafleur, M.; Silvius, J. R. *Biophys. J.* **1998**, *75*, 2900.
(26) Barentin, C.; Muller, P.; Joanny, J. F. *Macromolecules* **1998**, *31*, 2198.
(27) Wiesenthal, T.; Baekmark, T. R.; Merkel, R. *Langmuir* **1999**, *15*, 6837.
(28) Gallant, J.; Lavoie, H.; Tessier, A.; Munger, G.; Leblanc, R. M.; Salesse, C. *Langmuir* **1998**, *14*, 3954.
(29) Vranken, N.; Van der Auweraer, M.; De Schryver, F. C.; Lavoie, H.; Bélanger, P.; Salesse, C. *Langmuir* **2000**, *16*, 9518.
(30) Ducharme, D.; Tessier, A.; Russev, S. *Langmuir* **2001**, *17*, 7529.
(31) Kawaguchi, M.; Tohyama, M.; Mutoh, Y.; Takahashi, A. *Langmuir* **1988**, *4*, 407.
(32) Gaines, G. L., Jr. *Langmuir* **1991**, *7*, 834.
(33) Kawaguchi, M.; Tohyama, M.; Takahashi, A. *Langmuir* **1988**, *4*, 411.
(34) Nagata, K.; Kawaguchi, M. *Macromolecules* **1990**, *23*, 3957.
(35) Lee, K. Y. C.; Lipp, M. M.; Takamoto, D. Y.; Ter-Ovanesyan, E.; Zasadzinski, J. A. *Langmuir* **1998**, *14*, 2567.
(36) Esker, A. R.; Zhang, L.-H.; Sauer, B. B.; Lee, W.; Yu, H. *Colloids Surf., A* **2000**, *171*, 131.
(37) Carignano, M. A.; Szleifer, I. *Macromolecules* **1995**, *28*, 3197.
(38) de Gennes, P. G. *Adv. Colloid Interface Sci.* **1987**, *27*, 189.
(39) Wang, S.; Ramirez, J.; Chen, Y., Wang, P. G.; Leblanc, R. M. *Langmuir* **1999**, *15*, 5623.
(40) Seoane, R.; Miñones, J.; Conde, O.; Miñones, J., Jr.; Casas, M.; Iribarnegaray, E. *J. Phys. Chem. B* **2000**, *104*, 7735.
(41) Muñoz, M. G.; Monroy, F.; Ortega, F.; Rubio, R. G.; Langevin, D. *Langmuir* **2000**, *16*, 1083.
(42) Gopal, A.; Lee, K. Y. C. *J. Phys. Chem. B* **2001**, *105*, 10348.
(43) Gidalevitz, D.; Mindyuk, O. Y.; Stetzer, M. R.; Heiney, P. A.; Kurnaz, M. L.; Schwartz, D. K.; Ocko, B. M.; McCauley, J. P., Jr.; Smith, A. B., III *J. Phys. Chem. B* **1998**, *102*, 6688.
(44) Discher, B. M.; Schief, W. R.; Vogel, V.; Hall, S. B. *Biophys. J.* **1999**, *77*, 2051.
(45) Krüger, P.; Schalke, M.; Wang, Z.; Notter, R. H.; Dluhy, R. A.; Lösche, M. *Biophys. J.* **1999**, *77*, 903.
(46) Diamant, H.; Witten, T. A.; Gopal, A., Lee, K. Y. C. *Europhys. Lett.* **2000**, *52*, 171.
(47) Vogel, V.; Möbius, D. *J. Colloid Interface Sci.* **1988**, *126*, 408.
(48) Dynarowicz-Latka, P.; Dhanabalan, A.; Cavalli, A.; Oliveira, O. N., Jr. *J. Phys. Chem. B* **2000**, *104*, 1701.
(49) Seitz, M.; Struth, B.; Preece, J. A.; Plesnivy, T.; Brezesinski, G.; Ringsdorf, H. *Thin Solid Films* **1996**, *284−285*, 304.
(50) Vila Romeu, N.; Miñones Trillo, J.; Conde, O.; Casas, M.; Iribarnegaray, E. *Langmuir* **1997**, *13*, 71.
(51) Hughes, A. V.; Taylor, D. M.; Underhill, A. E. *Langmuir* **1999**, *15*, 2477.
(52) Vignaud, G.; Gibaud, A.; Wang, J.; Sinha, S. K.; Daillant, J.; Grübel, G.; Gallot, Y. *J. Phys. Condens. Matter* **1997**, *9*, L1.
(53) Gaines, G. L., Jr. *Insoluble monolayers at liquid−gas interfaces*; Wiley: New York, 1966.

MA0257806